Transactions, SMiRT-23
Manchester, United Kingdom - August 10-14, 2015
Division II, Paper ID 109
Fracture Mechanics and Structural Integrity

EXPERIMENTAL AND NUMERICAL INVESTIGATION OF THERMO MECHANICAL FATIGUE BEHAVIOUR OF FAST REACTOR TYPE 316 STAINLESS STEEL WITH AND WITHOUT DWELL TIME

Reza Hormozi[1], Farid Biglari[2], Kamran Nikbin[1]

[1] Department of Mechanical Engineering, Imperial College London, SW7 2AZ, UK
[2] Faculty of Mechanical Engineering, Amirkabir University of Technology, Tehran, Iran

ABSTRACT

Many advanced gas cooled reactor (AGR) power plant components with operating temperatures in the range of 500-650°C undergo creep-fatigue loading conditions which may lead to isothermal low cycle fatigue (LCF) and thermo mechanical fatigue (TMF) damages. Fully-reversed, strain controlled in-phase (IP) thermo-mechanical fatigue tests were conducted on the Type 316FR and the temperature was cycled between 500°C and 650°C for the strain ranges of $\Delta\varepsilon=\pm0.4\%$, $\pm0.8\%$, $\pm1.0\%$ and $\pm01.2\%$. A constitutive model based on isotropic and nonlinear kinematic hardening rules was used to replicate numerically the cyclic structural behaviour of the material until stabilisation. Finally to demonstrate the damage initiation and the damage evolution, a hysteresis energy-based phenomenological model was implemented in a user subroutine combined with a creep damage model based on the time-fraction law to replicate the experimental results. For the purpose of replicating the TMF behaviour of the material, the cyclic data obtained in isothermal tests at maximum and minimum temperatures were employed.

INTRODUCTION

This paper highlights the numerical investigations performed on the type 316FR material under Thermo Mechanical Fatigue conditions. The numerical results were then compared against the experimental results which were published in [1]. In the past few years, considerable amount of experimental tests have been carried out on austenitic stainless steels of 304, 316SS and their variants [2-12]. The experimental results cover two types of in-phase (IP) TMF tests which were conducted at the temperature range of 500°C-650°C with and without hold times at the maximum strains in tension and compression. The details of the test matrices and the mechanical strain-temperature waveform are as detailed in [1].

The evolution of the cyclic-stress response per cycle, the cyclic hysteresis loops and the evolution of the accumulated inelastic strain energy density per cycle for the strain ranges of $\Delta\varepsilon=\pm0.4\%$ to $\Delta\varepsilon=\pm1.2\%$ are used to identify the material properties and to determine the parameters required to predict the TMF behaviour numerically. The stress relaxation during the hold periods under TMF conditions, are also simulated and presented to demonstrate the effect of hold time and subsequently the effect of creep on the overall cyclic life behaviour of the material. The comparison of the numerical results against the experimental results can indicate the accuracy of the selected material properties.

Furthermore, to describe the failure stage, a hysteresis energy-based phenomenological model was developed to predict the fatigue damage initiation and evolution throughout the last stage of the material behaviour. This model was implemented in Abaqus via user defined sub-routine. The energy-based model has also been approached by other authors in [13, 14]. In an effort to study the interaction of creep and fatigue, the tests where the hold time introduced, the damage mechanism (initiation+evolution) needed to consider the time dependent damage factor i.e. the creep damage to more accurately replicate the material behaviour. Hence, the overall damage could be decomposed as following;

$$D_t = D_c + D_f \quad (1)$$

In which D_t, D_c, D_f are the total, creep and fatigue damage respectively. In the tests without hold time, the above expression can be expressed as $D_t = D_f$. For the tests where the hold time was introduced, i.e. the interrupted creep and varying frequency fatigue tests, the total damage model was assumed to follow the life fraction method as proposed by Taira [15]. This model, which is an empirical model, is based on the cumulative damage rules which assume that the life of the specimens is governed by the separated accumulation of the fatigue/time-independent and creep/time-dependent damages. In the developed user defined damage model sub-routine, the overall damage is assumed to follow the following expression. Detailed description of the proposed model is provided in [16].

$$D_{pc} = D_c + D_f = \int_0^{t_h} \frac{dt}{t_r} + (hysteresis\ energy\ damage) \quad (2)$$

EXPERIMENT

Material and specimen

The material used for this project is a type 316FR stainless steel. The same material as used in [1, 16] which is similar to type 316L (N). 316FR is a low-carbon grade of stainless steel with a more closely specified nitrogen content and chemistry optimized to enhance elevated-temperature performance. The samples were cylindrical hourglass which were designed and machined in accordance with the ASTM standards [17-19]. The middle section of the specimen is referred to as the gauge section which was at least 16mm in order to allow the placement of the extensometer ceramic arms which are 12.5mm apart. The specimen was designed to make sure the required temperature could be achieved.

Experimental results

Thermo mechanical fatigue tests were conducted on the same material and on the specimens with the geometry as shown previously in [1], where full details of the experimental procedures and their results can be found. The tested specimens with their reference numbers can be found in Table 1. The evolution of the maximum and minimum stresses recorded during the TMF tests with continuous cyclic loading (i.e. no hold time) and the tests with the introduction of hold time in maximum strains in tension and compression are presented in Figure 1and Figure 2 respectively for demonstration purpose. The three stages of initial hardening, stabilisation and damage evolution until failure can be noticed for all the TMF tests under both with and without hold time. Metallographic and fractographic investigations were conducted on the tested TMF samples to determine the microstructure of the samples tested at the temperature range of 500-650°C under both with and without hold time(i.e. f=0.001Hz and 0.01Hz respectively). The full details of this investigation can also be found in [1]

Table 1. Material reference details

Specimen reference	Mechanical strain range	Test	Temperature
[ref]	[%]	[-]	[C°]
316 FR28	±0.4	TMF	500-650
316 FR14	±0.8	TMF	500-650
316 FR12	±1.0	TMF	500-650
316 FR13	±1.2	TMF	500-650
316 FR27	±0.4	TMF	500-650
316 FR24	±0.8	TMF	500-650
316 FR23	±1.0	TMF	500-650

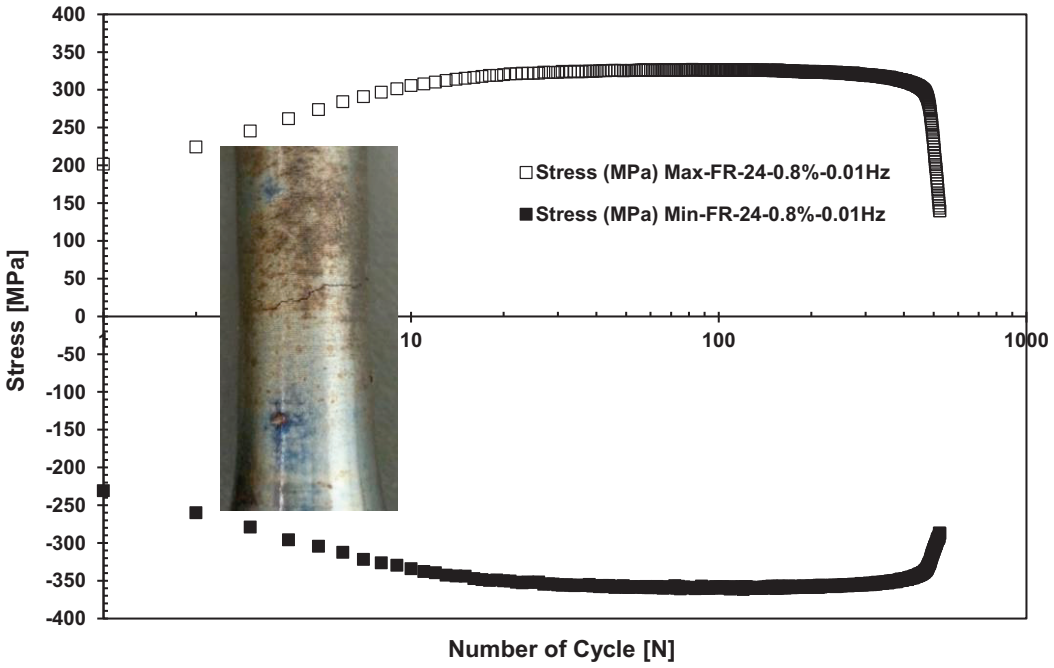

Figure 1: TMF Cyclic stress response for Δε=±0.8%, at 500-650°C with f=0.01Hz

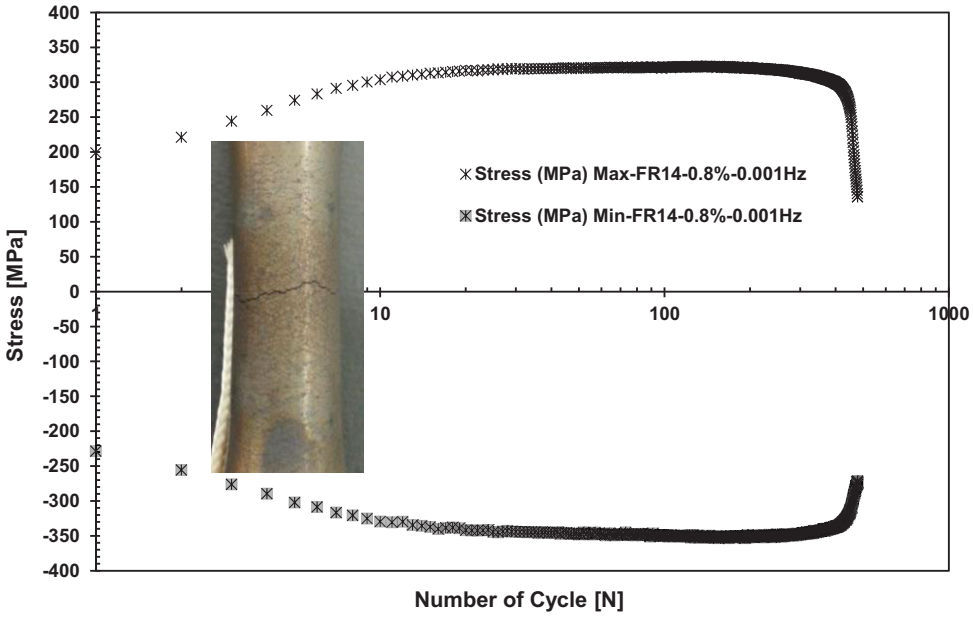

Figure 2: TMF Cyclic stress response for Δε=±0.8%, at 500-650°C with f=0.001Hz

CYCLIC PLASTICITY BEHAVIOUR

The cyclic plasticity and the time dependency behaviour of the material under strain-controlled temperature cyclic TMF tests, until steady-state condition (stabilised cycle) has been studied. The experimental data presented in [1] for LCF and TMF results are employed to determine a constitutive model that can replicate numerically the cyclic structural behaviour of the material. The isotropic and nonlinear kinematic hardening models are the same as those discussed in [16, 20] and the required parameters are derived for the finite element simulation purposes. Finally, the experimental LCF results are used in order to simulate the material behaviour under TMF condition.

TMF cyclic parameters

It is quite remarkable that majority of the low cycle fatigue (LCF) tests at elevated temperature that have been undertaken in the past forty years, relatively few have performed a test where the temperature as well as the mechanical strain range have varied. The argument in conducting LCF tests is to use the manipulated isothermal data to predict the service cycles of varying shape and magnitude which produces thermo mechanical (TMF) behaviour [21]. In order to simulate the TMF cyclic behaviour of the material similar to that observed in the experimental tests, the material properties obtained from the cyclic stress strain (CSS) isothermal LCF tests for the temperatures of 500°C and 650°C are used. Values of Young's modulus at each temperature were determined from the linear unloading part of the hysteresis loops (i.e. the average of elastic tension and compression arms).
As for simulating the cyclic plasticity and hardening behaviour under TMF conditions, due to high level of dependency of parameters to testing conditions, using the material parameters in the Lemaitre and Chaboche model [22] would require an optimisation procedure to obtain the suitable values. The gradient-based Levenberg-Marquardt method [23-25] is often used for this purpose which determines the first optimum set of the parameters using the initial set of material parameter estimates. However, in the view of simulating the TMF behaviour of the material investigated here, a direct method to use the isothermal LCF test data from a stabilised cycle for the temperature range of 500°C and 650°C is approached.

Nonlinear Isotropic/Kinematic hardening component

The change in the size of the yield surface is characterised by the variation of the equivalent stress $\boldsymbol{\sigma^0}$ which is a function of the equivalent plastic strain $\bar{\boldsymbol{\varepsilon}}^{\boldsymbol{pl}}$ of the material. The translation of the yield surface in the stress space through the backstress $\alpha_{*\mathrm{k}}$, is identified by the definition of the nonlinear kinematic hardening component. These two models are fully discussed in the work published in [16, 20, 26]. This behaviour could also be observed by the manifestation of the Bauschinger effect when the load is reversed. Figure 3 shows the comparison of the stabilised cycles of the in-phase TMF test result for the temperature range of 500-650° with the isothermal LCF test results conducted under mechanical strain range of ±0.4% at 500 and 650°C. It can be observed that the maximum and the minimum stress values for the TMF test appear to be similar to the stress values of the isothermal test data at the top and the bottom of the stabilised cycles. Therefore, this could indicate the fact that the definition of the cyclic hardening and plasticity, i.e. nonlinear isotropic/kinematic hardening parameters, for the TMF tests can be based on the parameters determined from the tests conducted under isothermal LCF tests for the mechanical strain ranges considered here.

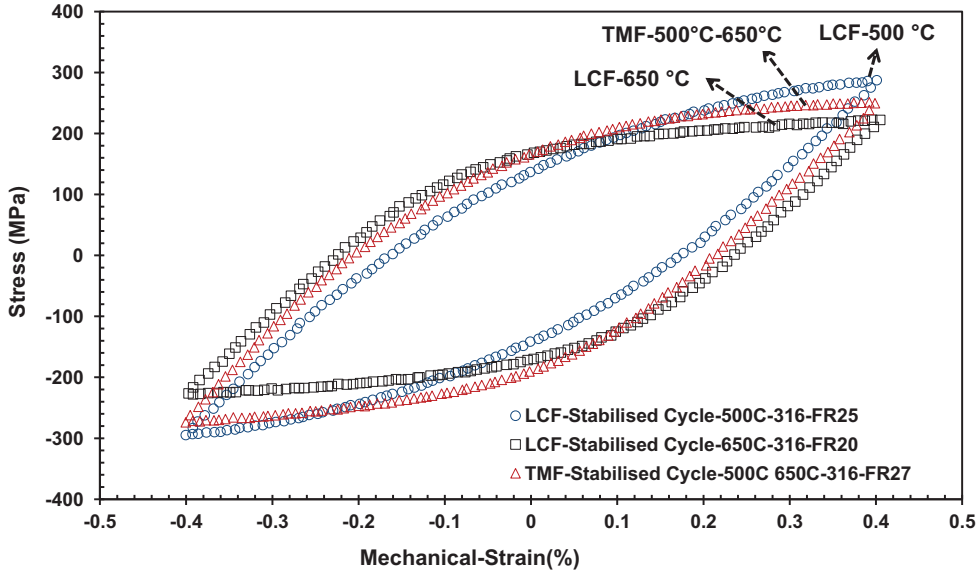

Figure 3: Comparison of stabilised cycles of isothermal LCF tests at 500 and 650°C with TMF test at the temperature range of 500-650°C with Δε=±0.4%, f=0.01Hz

Thermal expansion

As the material is heated up to an elevated temperature, thermal expansion takes place which remains almost constant during the isothermal LCF tests and it increases or decreases where the temperature varies in a range. In order to demonstrate this behaviour in the FE simulations, the thermal expansion coefficients, α , as well as the thermal conductivity parameters, χ, are defined for the temperatures the tests were conducted at. The thermal parameters documented in the physical properties section of the R66 [27] for austenitic stainless steels are summarised in
Table **2** and
Table **3**. These parameters are defined using equations (3) and (4). Additionally, by using equation (3), the thermal expansion coefficients for the TMF tests conducted for the temperature range of 500-650°C are determined from the experimental data, to compare with the R66 material properties. At 650°C the material yielded a coefficient of thermal expansion of 21.04 x10^{-6} °C $^{-1}$ while at 500°C this was 20.22 x10^{-6} °C $^{-1}$ which both were within the suggested uncertainty of ± 2.8 x 10^{-6}°C $^{-1}$ as specified in R66 [27]. This discrepancy in the results could also be justified with the fact that the thermal expansion coefficient for the specimen gauge itself cannot necessarily be an indicator of a true value from the thermal signal, since it may contain the response of the stabilised extensometer detection unit and the ceramic legs during cycling.

$$\alpha = 15.3 + 0.839 \times 10^{-2}\,\theta \quad \textbf{(3)}$$

$$x = 13.65 + 0.1434\,x\,10^{-1}\,\theta \quad \textbf{(4)}$$

Table 2. Thermal Conductivity of Austenitic Stainless Steels

Temperature °C	20	100	200	300	400	500	600	700
χ, Wm^{-1} °C^{-1}	13.9	15.1	16.5	18.0	19.4	20.8	22.3	23.7

Table 3. Coefficient of Thermal Expansion of Austenitic Stainless Steels

Temperature °C	20	100	200	300	400	500	600	700
α , 10^{-6} °C $^{-1}$	15.5	16.1	17.0	17.8	18.7	19.5	20.3	21.2

DAMAGE ACCUMULATION

The measurement of the experimental damage of the material under cyclic tests is discussed in [16] where is it agreed that equation (5) is more suitable for this purpose.

$$D_i = 1 - \frac{E_i}{E'} \tag{5}$$

A damage initiation method using the hysteresis energy per cycle is employed to incorporate damage initiation analysis into TMF condition. This phenomenological damage initiation model predicts the initiation of damage for the ductile materials subjected to cyclic load in association with the accumulation of inelastic strain energy density per cycle, Δw, which has been previously described in [16, 20]. The damage initiation model follows the following equation;

$$N_0 = r_1 \Delta w_{sta}^{r_2} \tag{6}$$

The damage evolution model for the tests without hold time is based on method described in [16, 20], in which the power law damage evolution model is employed to accommodate material degradation once the damage is initiated. The rate of damage, D , per cycle, N, for a material point can therefore be defined as;

$$\frac{dD}{dN} = \frac{r_3 \Delta w_{avg}{}^{r_4}}{G} \tag{7}$$

The damage evolution model for the tests with hold time is thoroughly described in the work presented in [16] where the combination of time fraction creep damage model as well as the damage evolution for tests under cyclic loads are emerged to provide a unique model that can represent the overall damage evolution under creep-fatigue condition. This was shown earlier in equation (2).

FE RESULTS AND DISCUSSIONS

The material behavior is simulated using the commercial Finite Element software, Abaqus, for the first two cyclic phases of the overall behavior, i.e. cyclic hardening and stabilization as well as the damage evolution under both with and without hold time. The simulation results are also compared with the experimental results to verify the validity of the FE modeling. A 2D axisymmetric model with a 4mm of radius and a 6.25mm height was meshed using six first order CAX4R axisymmetric quadrilateral reduced integration elements as described in [16]. Comparisons are made between the experimental and numerical results including first and stabilised cyclic stress-strain loopsand stress relaxation at selected strain levels for the tests conducted with dwell period (450 s strain hold) where creep and fatigue interaction may be expected. The FE results for the TMF tests with continuous cyclic loading at strain ranges of ±0.8% presented in Figure 4, whereas the numerical results for the tests with dwell period at strain ranges of ±0.8% are illustrated in Figure 5. Using the creep data summarised in [16], the stress relaxation history in the first and stabilised cycles for the TMF tests with hold time are demonstrated in Figure 6. The FE results showed that the material properties derived for the nonlinear isotropic/kinematic hardening components could represent the material behaviour; however it must be noted that the comparison of the stabilised hysteresis loops indicated that the maximum stresses in tension do not fully match the experimental results. This is due to the fact which was observed earlier in Figure 3.

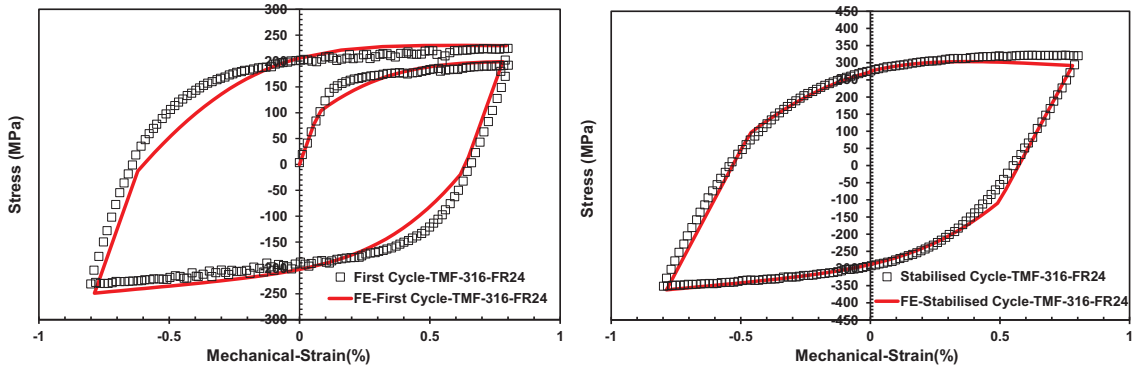

Figure 4: First-Stabilised loops, TMF tests, 500-650°C, Δε=±0.8%, f=0.01Hz

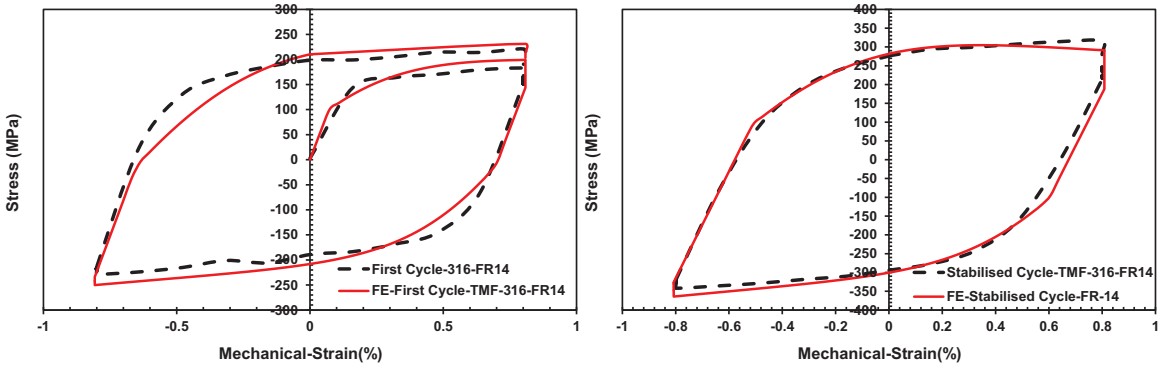

Figure 5: First-Stabilised loops, TMF tests, 500-650°C, Δε=±0.8%, f=0.001Hz

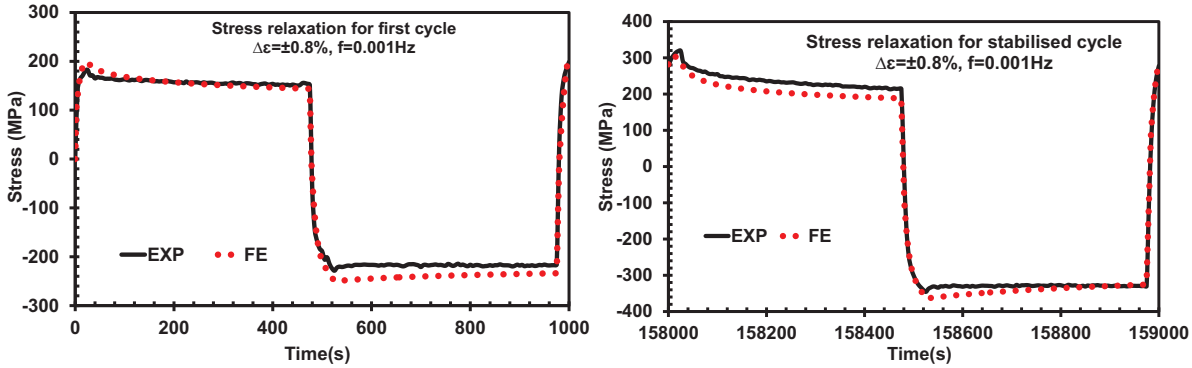

Figure 6: stress relaxation of First-Stabilised loops for the TMF tests at 500-650°C with Δε=±0.8%

The damage initiation data set $(N_0, \Delta w_{sta})$ for the TMF tests are shown in Figure 7 in which the constants for the tests with hold time are defined as r_1 = 1735.4, r_2 = -1.239 and in the tests without hold time these constants are as r_1 = 2153.5 and r_2 = -1.732. However for the TMF tests, for fatigue proportion of the tests with hold time, the parameters are determined as r_3=2.40E-5, r_4= 0.743 and for TMF tests without hold time these parameters are as r_3=2.401E-5 and r_4= 0.746 as shown in Figure 8 a) and b) respectively. For the tests with hold time, the CREEP user-defined subroutine was employed in combination with the USDFLD. The CREEP subroutine was modified in order to implement the stress relaxation behaviour using the primary and the secondary creep properties along with the creep damage method as detailed in [16] and shown below.

$$D_c = \lambda \times \int_0^{t_h} \frac{dt}{t_r} = \lambda \times \sum \frac{\Delta t_h}{t_r} \qquad \textbf{(8)}$$

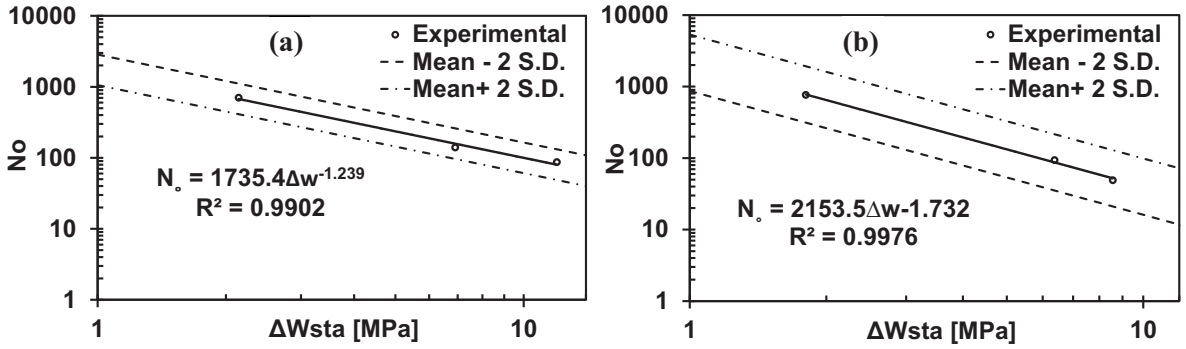

Figure 7: Damage initiation parameters for a) TMF, f=0.001Hz and b) TMF, f=0.01Hz

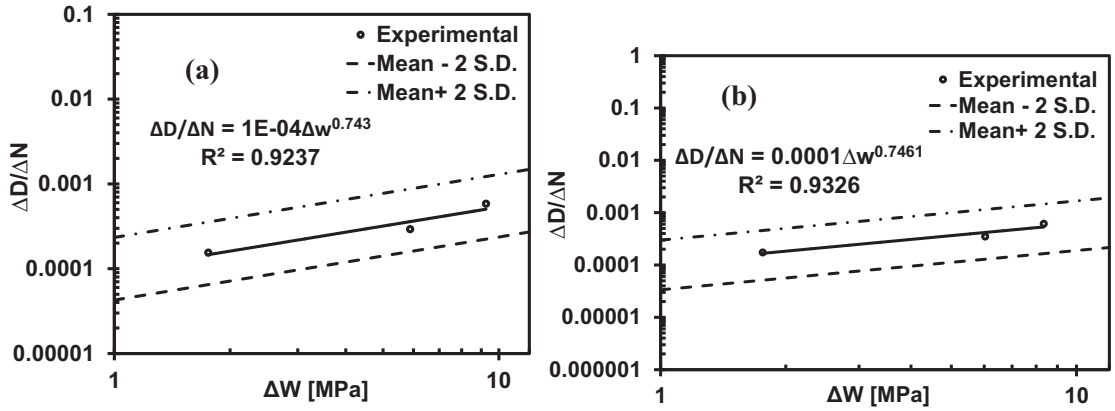

Figure 8: Decomposed fatigue damage evolution parameters for TMF tests a) with hold time b) without

The FE simulations of the tests with 10% failure criterion were conducted and compared against the experimental results as when the damage initiated. In order to assess the accuracy of the FE results, the evolution of the total damage evolution (D_t), creep and fatigue damages (D_c , D_f) are presented as following.

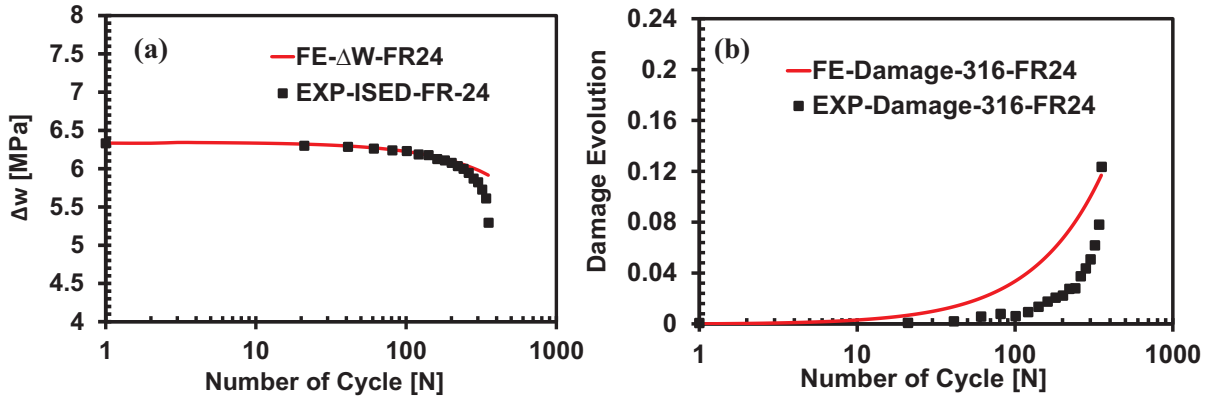

Figure 9: FE & Experimental (a) Inelastic strain energy density evolution, Δw (b) Total damage based on hysteresis energy, TMF tests, 500-650°C with Δε=±0.8%,f=0.01Hz

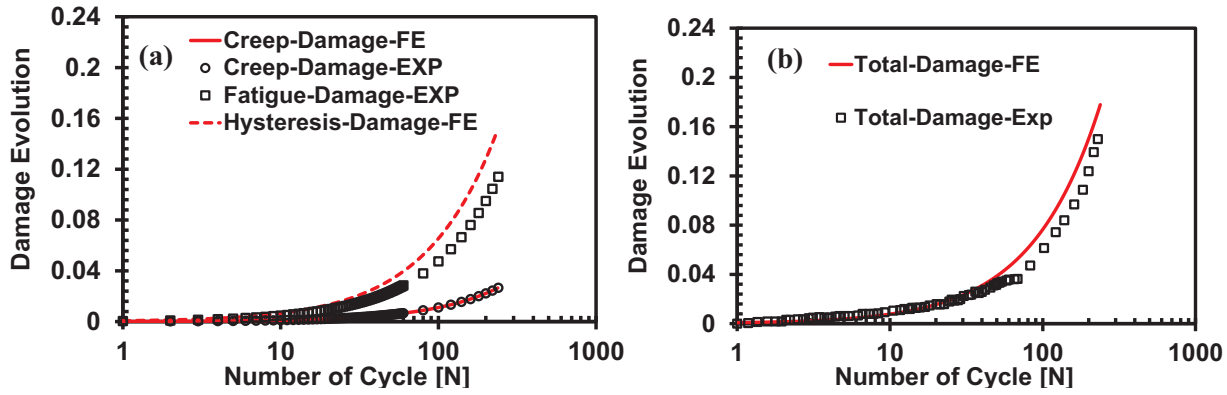

Figure 10: FE & Experimental (a) Cree-Fatigue damages, (b) Total damage for TMF tests, 500-650°C with $\Delta\varepsilon=\pm 0.8\%$, f=0.001Hz

CONCLUSION

The material behaviour for the three stages of *cyclic hardening, stabilisation and failure* for the LCF tests conducted under strain-controlled condition with and without hold time at the temperature of 650°C was analysed and replicated numerically. By using the nonlinear isotropic/kinematic hardening models in combination with the hysteresis energy-based phenomenological damage model (for the tests with continuous cyclic loading) and the proposed creep-fatigue damage model (i.e. the time fraction and the hysteresis damage models for the tests with hold time) the following conclusions can be drawn;

- The temperature dependent Abaqus nonlinear isotropic/kinematic hardening model proved to be a reasonably good model to simulate the material behaviour of 316FR under TMF conditions.
- The application of hysteresis energy in characterising the damage initiation and evolution was proved to be valid for the TMF tests with and without hold time.
- The damage model based on the energy in the hysteresis loops was implemented in the subroutine and the comparison of the FE simulations and the experimental results for the LCF tests without hold time indicate the suitability of this method.
- Moreover, as shown in Figure 10, good agreement can be observed between the experimental results and the FE simulations for the tests in which the hold time was introduced. This highlights the effectiveness of combining the time-fraction (creep) and hysteresis energy method (fatigue) to represent the material behaviour

REFERENCES

1. Hormozi, R., F. Biglari, and K. Nikbin, Experimental study of type 316 stainless steel failure under LCF/TMF loading conditions. *International Journal of Fatigue*, 2015. **75**(0): p. 153-169.
2. Zauter, R., et al. Thermomechanical fatigue of the austenitic stainless steel AISI 304L. in *ASTM Special Technical Publication*. 1993.
3. Zauter, R., H.J. Christ, and H. Mughrabi, Some aspects of thermomechanical fatigue of AISI 304L stainless steel: Part I. creep- fatigue damage. *Metallurgical and Materials Transactions A*, 1994. **25**(2): p. 401-406.
4. Shi, H.-J., Z.-G. Wang, and H.-H. Su, Thermomechanical fatigue of a 316L austenittc steel at two different temperature intervals. Scripta Materialia, 1996. **35**(9): p. 1107-1113.
5. Kuwabara, K. and A. Nitta, THERMAL-MECHANICAL LOW-CYCLE FATIGUE UNDER CREEP-FATIGUE INTERACTION ON TYPE 304 STAINLESS STEELS. *Fatigue & Fracture of Engineering Materials & Structures*, 1979. **2**(3): p. 293-304.
6. Maier, H.J. and H.J. Christ, Modeling of cyclic stress-strain behavior and damage mechanisms under thermomechanical fatigue conditions. *International Journal of Fatigue*, 1997. **19**(SUPPL.1): p. S267-S274.

7. Shi, H.J. and G. Pluvinage, Cyclic stress-strain response during isothermal and thermomechanical fatigue. *International Journal of Fatigue*, 1994. **16**(8): p. 549-557.
8. Yoshihisa, E. and S. Ganesh Sundara Raman, Thermomechanical and isothermal fatigue behaviour of type 316 stainless steel base metal, weld metal, and joint. *Science and Technology of Welding and Joining*, 2000. **5**(3): p. 174-182.
9. O'Donnell, M.P., R.C. Hurst, and D. Taylor, Observations of the micromechanisms affecting the fracture path for thermal fatigue-creep loading of a 316L stainless steel. *Materials at High Temperatures*, 1998. **15**(2): p. 95-98.
10. Robertson, C., M.C. Fivel, and A. Fissolo, Dislocation substructures in 316L stainless steel under thermal fatigue up to 650 K. *Materials Science and Engineering A*, 2001. **315**(1-2): p. 47-57.
11. Rau, K., T. Beck, and D. Löhe, Isothermal, thermal-mechanical and complex thermal-mechanical fatigue tests on AISI 316 L steel-a critical evaluation. *Materials Science and Engineering A*, 2003. **345**(1-2): p. 309-318.
12. Nagesha, A., et al., Thermomechanical fatigue evaluation and life prediction of 316L(N) stainless steel. *International Journal of Fatigue*, 2009. **31**(4): p. 636-643.
13. Darveaux, R. Effect of simulation methodology on solder joint crack growth correlation. in *Electronic Components & Technology Conference*, 2000. 2000 Proceedings. 50th. 2000.
14. Lau, J.H., S.H. Pan, and C. Chang, A new thermal-fatigue life prediction model for wafer level chip scale package (WLCSP) solder joints. *Journal of Electronic Packaging*, 2002. **124**(3): p. 212-220.
15. Taira, S., Lifetime of structures subjected to varying load and temperature, Creep in structures. Springer-verlag, 1962: p. 96-124.
16. Hormozi, R., F. Biglari, and K. Nikbin, Experimental and numerical creep–fatigue study of Type 316 stainless steel failure under high temperature LCF loading condition with different hold time. *Engineering Fracture Mechanics*, 2015. **141**(0): p. 19-43.
17. E606–04, Standard Practice for Strain-Controlled Fatigue Testing. 2004, ASTM International: Annual Book of ASTM Standards.
18. E2368-10, Standard Practice for Strain Controlled Thermomechanical Fatigue Testing. 2010, ASTM International: Annual Book of ASTM Standards.
19. E2714–09, Standard Test Method for Creep-Fatigue Testing. 2009, ASTM International: Annual Book of ASTM Standards.
20. Hormozi, R., F. Biglari, and K. Nikbin, Taguchi sensitivity analysis of damage parameters for predicting the damage Mechanism of 9Cr steel under low-cycle fatigue test. *Fatigue & Fracture of Engineering Materials & Structures*, 2014: p. n/a-n/a.
21. Skelton, R.P., et al., Modelling thermo-mechanical fatigue hysteresis loops from isothermal cyclic data. ASTM special technical publication, 2000. **1371**: p. 69-84.
22. Lemaitre, J., and Chaboche J.L. ,, Mechanics of Solid Materials. *Cambridge University Press*, 1990.
23. Fossum, A., Rate data and material model parameter estimation. *Journal of engineering materials and technology*, 1998. **120**(1): p. 7-12.
24. Fossum, A., Parameter estimation for an internal variable model using nonlinear optimization and analytical/numerical response sensitivities. *Journal of engineering materials and technology*, 1997. **119**(4): p. 337-345.
25. Marquardt, D.W., An algorithm for least-squares estimation of nonlinear parameters. *Journal of the Society for Industrial & Applied Mathematics*, 1963. **11**(2): p. 431-441.
26. Hormozi, M.R., F. Biglari, and K.M. Nikbin. Investigation of Stress Stabilization Behavior of Type 316 Steel. in ASME 2013 *Pressure Vessels and Piping Conference*. 2013. American Society of Mechanical Engineers.
27. Hamm, C.D., AGR Materials Data Handbook-Section 2, Physical Properties. 2011, British Energy Generation Ltd.